Coherence properties from speckle contrast analysis at the European XFEL

Journal of Physics: Conference Series **2380** (2022) 012085 doi:10.1088/1742-6596/2380/1/012085

Coherence properties from speckle contrast analysis at the European XFEL

F Dallari[1], I Lokteva[1,2], J Möller[3], A Jain[1], W Roseker[1], F Westermeier[1], C Goy[1], U Boesenberg[3], J Hallmann[3], A Rodriguez-Fernandez[3], M Scholz[3], R Shayduk[3], A Madsen[3], G Grübel[1,2] and F Lehmkühler[1,2]

[1]Deutsches Elektronen-Synchrotron DESY, Notkestr. 85, 22607 Hamburg, Germany
[2]The Hamburg Centre for Ultrafast Imaging, Luruper Chaussee 149, 22761 Hamburg, Germany
[3]European X-Ray Free-Electron Laser Facility, Holzkoppel 4, 22869 Schenefeld, Germany

E-mail: felix.lehmkuehler@desy.de

Abstract. We show the results of speckle contrast analysis at the MID instrument of European XFEL in the hard X-ray regime. Speckle patterns measured from static colloidal samples are compared to results previously obtained at the SPB/SFX instrument. A high degree of coherence of 0.79 is obtained by modelling the q-dependence of the speckle contrast, that corresponds to a number of coherent modes of $M = 1.7$. Furthermore, the variation of contrast over many pulse trains is exceptional low, resulting in a degree of coherence with a relative standard deviation below 0.1. Our results demonstrate the high stability of coherence properties at European XFEL over many X-ray pulses and pulse trains which is a prerequisite for coherence-based techniques such as MHz X-ray photon correlation spectroscopy.

1. Introduction

New X-ray facilities such as free-electron lasers (FEL) and the next-generation of synchrotron radiation sources provide high-intensity hard X-rays with a high degree of coherence [1, 2, 3, 4]. This enables coherent scattering and imaging experiments such as coherent diffractive imaging (CDI), ptychography as well as X-ray photon correlation spectroscopy (XPCS) with unprecedented spatial and temporal resolution. The successful application of these techniques depends critically on the coherence properties of the X-ray beam. When a (partially) coherent X-ray beam is scattered by a sample, a speckle pattern, i.e. a grainy diffraction pattern, is obtained. As the positions of all scattering objects are encoded in this speckle pattern, the structure of the sample can be obtained in many cases by CDI and ptychography [5, 6, 7, 8, 9]. On the other hand, if the sample structure changes, the speckle pattern will change accordingly and the sample dynamics can be accessed by intensity-intensity correlations in the framework of XPCS [10, 11, 12].

The coherence properties of the X-ray beam can be described by the mutual coherence function of the electromagnetic field [7]. The measured quantity is intensity I, hence the lowest order coherence function experimentally accessible is of second order. The second-order degree

of coherence is given by the normalized variance of intensity on the detector as

$$\gamma_2 \equiv \frac{1}{M} = \frac{\langle I^2 \rangle - \langle I \rangle^2}{\langle I \rangle^2}, \tag{1}$$

with the number of coherent modes M. Following the Siegert relation, the first-order degree of coherence is given by [7]

$$\gamma_1 = \sqrt{\gamma_2}. \tag{2}$$

The degree of coherence can be obtained from coherent scattering experiments by calculating the speckle contrast β. This is done either following Eq. 1 for different wave vector transfers $\mathbf{q}$, with modulus $q = |\mathbf{q}| = \frac{4\pi}{\lambda} \sin(\theta/2)$, where λ is the photon wavelength and θ the scattering angle, or by analysing the intensity distribution [13]. At low count rates, the intensity distribution follows a negative binomial function [13, 14], and the momentum analysis of the negative-binomial distribution results in [15]

$$\beta_{\mathrm{exp}}(q) = \frac{\langle I^2(q) \rangle - \langle I(q) \rangle^2}{\langle I(q) \rangle^2} - \frac{1}{\langle I(q) \rangle} \tag{3}$$

for the speckle contrast. Besides the degree of coherence, the experimental speckle contrast β_{exp} depends on further properties, such as scattering geometry, beam size and detector pixels size [14, 16]. It can be written as

$$\beta_{\mathrm{exp}}(q) = \beta_{\mathrm{tr}} \beta_{\mathrm{rad}} \beta_{\mathrm{det}}. \tag{4}$$

Following [14], β_{rad} considers the non-zero radial resolution and depends on the energy band width, sample dimensions and beam geometry, while β_{det} describes the contrast reduction due to the detector resolution. Thus, β_{tr} is a measure of the transverse coherence. The degree of coherence is thus given by

$$\gamma_1 = \sqrt{\beta_{\mathrm{tr}}}. \tag{5}$$

Previous experiments at FEL sources measured the speckle contrast and thus the degree of coherence by means of analysing speckle patterns from static scatterers [2, 16, 17, 18]. At the SPB/SFX instrument of European XFEL [19], we found a high degree of coherence with low pulse-to-pulse fluctuations [20]. Furthermore, speckle contrasts obtained from single-pulse patterns matched the ones from correlating a series of speckle patterns, demonstrating a high stability of the beam parameters. Here we will extend and compare this study to recent results obtained at the Materials Imaging and Dynamics (MID) instrument [21] which is particularly dedicated to coherence-based techniques such as imaging and XPCS.

2. Experimental

Speckle patterns were measured at the MID instrument at the European XFEL [21]. The photon energy was 9 keV. The Adaptive Gain Integrating Pixel Detector (AGIPD) was placed 7.3 m downstream the sample in small-angle scattering geometry. Using the compound refractive lenses close to the sample position [21] the SASE beam was focused to 10×10 μm^2 at the sample position. As sample we used a dried powder of commercially-available spherical silica particles (Ludox, Sigma-Aldrich) of 15 nm radius filled to quartz capillaries of 1.5 mm thickness.

Speckle patterns were measured from 400 X-ray pulse trains with 200 X-ray pulses each. The pulse repetition rate was 2.256 MHz within the train, whereas the train repetition rate was 10 Hz. The sample was moved between the trains in order to avoid radiation damage. More experimental details can be found in [22], further details on the data processing with AGIPD are given in [23].

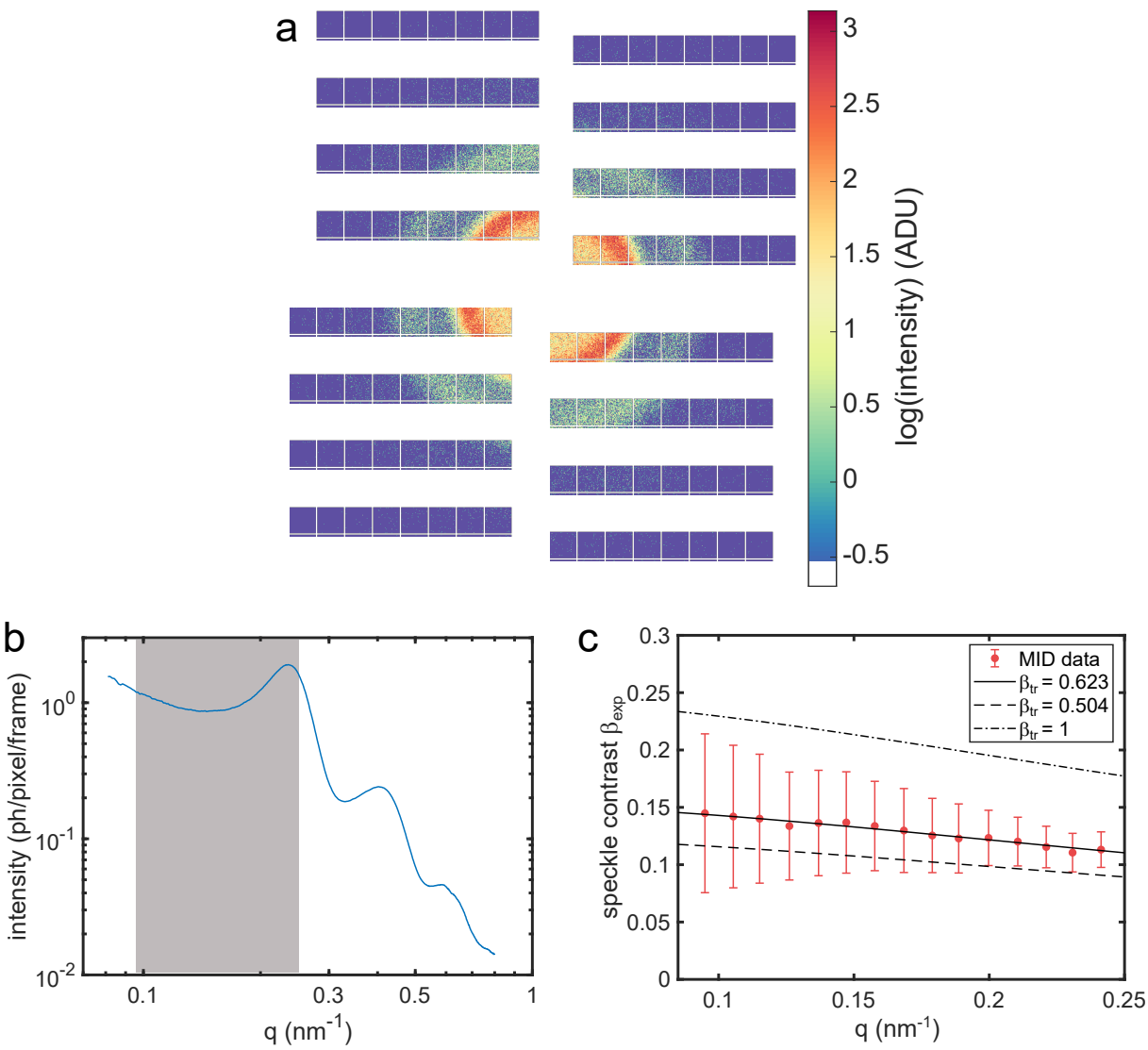

Figure 1. (a) Pedestal and common-mode corrected [23] single-pulse speckle pattern. The intensity is given in logscale of ADU (analog-digital unit) as detector output. (b) Intensity $I(q)$ averaged over all patterns. (c) q-dependence of speckle contrast β_{exp} averaged over 79300 speckle patterns. The error bars represent the standard deviation of β_{exp}. Continuous, dashed and dash-dotted lines are calculated following [14] with different values of β_{tr}.

3. Results

The speckle contrast was determined for single pulse patterns following Eq. 3. An exemplary single-pulse speckle pattern measured by the AGIPD is shown in Fig. 1 (a), the mean integrated intensity $I(q)$ is shown in Fig. 1 (b) of all 79300 speckle patterns analyzed. The grey area marks the q-region for which the speckle contrast was calculated. Here, the intensity is almost constant so that its varying influence on the speckle contrast can be neglected. The average contrast from 79300 pulses is shown in Fig. 1 (c) as a function of q. Taking beam geometry, wave length, bandwidth and the experimental setup into account [14] using Eq. 4, we find a very good match for the q-dependence with $\beta_{\mathrm{tr}} = 0.623$, corresponding to $\gamma_2 = 0.79$. For comparison, at SPB/SFX we found a slightly lower degree of coherence of $\gamma_2 = 0.70$ [20]. Notably, the MID instrument is optimized for coherence applications which may explain its higher degree of

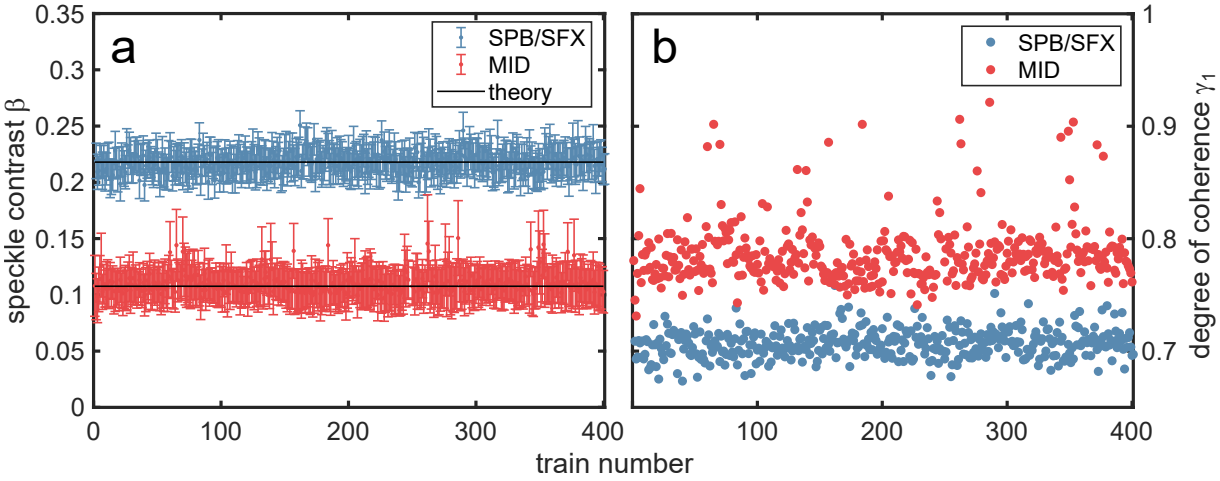

Figure 2. (a) Speckle contrast for $q = 0.23$ nm^{-1} from SPB/SFX [20] and MID averaged over all pulses from a train. The error bars represent the standard deviation. Black lines are theory values [14] as described in the text. (b) Degree of coherence from data shown in (a). For better visibilty the error bars are omitted.

coherence. This difference can also be attributed to different FEL operation modes as well as the different optics, e.g., different focussing schemes, used at both instruments.

Fig. 2 (a) compares speckle contrast values averaged over the pulse trains from SPB/SFX [20] and MID. At both instruments, the contrast is stable over all trains, and the standard deviation σ, representing the variation of contrast within a train, does not vary much. Due to the smaller beam size of about 4 μm used in the experiment at SPB/SFX [20], the speckle contrast is larger than for the MID experiment. As the setup and beam properties differ between the two instruments, we extract the degree of coherence γ_1 using Eq. 4. The results are shown in Fig. 2 (b). As discussed above, we find a slightly higher degree of coherence at MID around 0.79, with some outliers exceeding even 0.9.

The variation of speckle contrast on a pulse-to-pulse basis is further investigated in Fig. 3. Therein, histograms of single pulse speckle contrast measured at $q = 0.23$ nm^{-1} are compared again for both instruments, SPB/SFX and MID. The distribution of contrast was then modelled by both a Gaussian and a Gamma distribution. The two models describe the contrast distribution well for the SPB/SFX data, however the tails are better matched by the Gamma distribution. We obtain root mean squared errors (rmse) R of $R_{\mathrm{SPB,Gauss}} = 0.415$ and $R_{\mathrm{SPB,Gamma}} = 0.242$. The MID data could be best described by a Gaussian ($R_{\mathrm{MID,Gauss}} = 0.415$) except for $\beta_{\mathrm{exp}} > 0.14$ where the high-coherence outliers can be found. The Gamma distribution can model these values ($R_{\mathrm{MID,Gamma}} = 0.499$), but does not describe the overall shape of the distribution.

We find average values $\langle\beta\rangle_{\mathrm{SPB}} = 0.213$ and $\langle\beta\rangle_{\mathrm{MID}} = 0.108$. Remarkably, the widths of the distribution is similar for both instruments. This may suggest that this variation is an intrinsic property of the European XFEL. In general, such pulse-to-pulse variations of speckle contrast are expected because of the SASE nature of the FEL radiation and have been reported from other FEL facilities as well [2, 16, 17, 18, 24]. However, the data discussed here show a very small pulse-to-pulse variation compared to other facilities [16, 18, 24]. With respect to the degree of coherence we find mean and standard variations of $\langle\gamma_1\rangle_{\mathrm{SPB}} = 0.685 \pm 0.034$ and $\langle\gamma_1\rangle_{\mathrm{MID}} = 0.771 \pm 0.068$, respectively, for the studied wave vector transfer $q = 0.23$ nm^{-1}. This corresponds to average mode numbers of $M_{\mathrm{SPB}} = 2.1 \pm 0.2$ and $M_{\mathrm{MID}} = 1.7 \pm 0.3$. Furthermore, the degree of coherence varies less than 10% over many X-ray pulses. Note that the width of

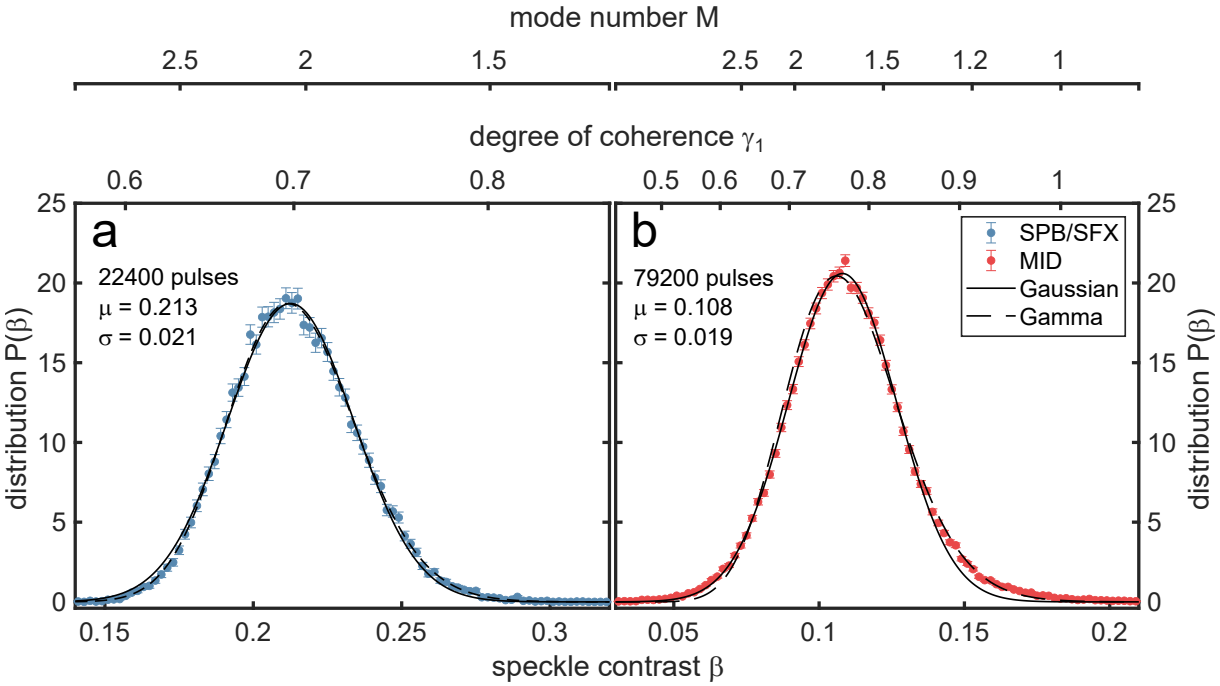

Figure 3. Histogram of speckle contrasts measured at $q = 0.23$ nm^{-1} from 22400 pulses at SPB/SFX (a) and 79300 pulses at MID (b). For comparison, γ_1 and M-axes are given on top and both Gaussian and Gamma distributions are fitted to the data. The values μ (mean) and σ (standard deviation) are given for a Gaussian distribution.

the distribution for this data set does not change with more pulses, thus representing its real value without significant influence from counting statistics.

4. Conclusion

We have shown a speckle contrast analysis at the MID instrument of European XFEL. The results have been compared to data we took previously in a similar experiment at the SPB/SFX instrument [20]. We found a high degree of coherence of 0.79 by modelling the q-dependence of the speckle contrast. The variation of contrast over many pulses is exceptional low (< 8 %). This high stability of coherence properties is crucial for MHz XPCS and X-ray speckle visibility experiments that rely on low pulse-to-pulse variations [12, 20, 22]. The remaining width in the distribution of speckle contrasts can be attributed to the SASE nature of the FEL radiation, resulting in spikes in the X-ray energy spectrum which is unique for each pulse. Therefore, it will be interesting to perform such studies using other operation modes such as self-seeded [25] or monochromatized radiation where maximum a few spikes hit the sample, thus minimizing the impact of the energy bandwidth on the speckle contrast and its variance.

Acknowledgments

We acknowledge European XFEL in Schenefeld, Germany, for provision of X-ray free-electron laser beamtime at Scientific Instrument MID (Materials Imaging and Dynamics) and would like to thank the staff for their assistance. This work is supported by the Cluster of Excellence 'Advanced Imaging of Matter' of the Deutsche Forschungsgemeinschaft (DFG) - EXC 2056 - project ID 390715994. We also acknowledge the scientific exchange and support of the Centre for Molecular Water Science (CMWS).

References

[1] Vartanyants I A, Singer A, Mancuso A P, Yefanov O M, Sakdinawat A, Liu Y, Bang E, Williams G J, Cadenazzi G, Abbey B, Sinn H, Attwood D, Nugent K A, Weckert E, Wang T, Zhu D, Wu B, Graves C, Scherz A, Turner J J, Schlotter W F, Messerschmidt M, Lüning J, Acremann Y, Heimann P, Mancini D C, Joshi V, Krzywinski J, Soufli R, Fernandez-Perea M, Hau-Riege S, Peele A G, Feng Y, Krupin O, Moeller S and Wurth W 2011 *Phys. Rev. Lett.* **107** 144801
[2] Gutt C, Wochner P, Fischer B, Conrad H, Castro-Colin M, Lee S, Lehmkühler F, Steinke I, Sprung M, Roseker W, Zhu D, Lemke H, Bogle S, Fuoss P H, Stephenson G B, Cammarata M, Fritz D M, Robert A and Grübel G 2012 *Phys. Rev. Lett.* **108** 024801
[3] Eriksson M, van der Veen J F and Quitmann C 2014 *J. Synchrotron Radiat.* **21** 837–842
[4] Weckert E 2015 *IUCrJ* **2** 230–245
[5] Williams G J, Quiney H M, Peele A G and Nugent K A 2007 *Phys. Rev. B* **75** 104102
[6] Thibault P, Dierolf M, Menzel A, Bunk O, David C and Pfeiffer F 2008 *Science* **321** 379–382
[7] Nugent K A 2010 *Adv. Phys.* **59** 1–99
[8] Miao J, Ishikawa T, Robinson I K and Murnane M M 2015 *Science* **348** 530–535
[9] Pfeiffer F 2017 *Nat. Photonics* **12** 9–17
[10] Madsen A, Fluerasu A and Ruta B 2018 Structural dynamics of materials probed by x-ray photon correlation spectroscopy *Synchrotron Light Sources and Free-Electron Lasers* (Springer International Publishing) pp 1989–2018 ISBN 978-3319143934
[11] Sandy A R, Zhang Q and Lurio L B 2018 *Annu. Rev. Mater. Res.* **48** 167–190
[12] Lehmkühler F, Roseker W and Grübel G 2021 *Appl. Sci.* **11** 6179
[13] Goodman J 2020 *Speckle phenomena in optics : theory and applications* (Bellingham, Washington: SPIE Press) ISBN 978-1510631489
[14] Hruszkewycz S O, Sutton M, Fuoss P H, Adams B, Rosenkranz S, Ludwig K F, Roseker W, Fritz D, Cammarata M, Zhu D, Lee S, Lemke H, Gutt C, Robert A, Grübel G and Stephenson G B 2012 *Phys. Rev. Lett.* **109** 185502
[15] Li L, Kwaśniewski P, Orsi D, Wiegart L, Cristofolini L, Caronna C and Fluerasu A 2014 *J. Synchrotron Radiat.* **21** 1288–1295
[16] Lehmkühler F, Gutt C, Fischer B, Schroer M A, Sikorski M, Song S, Roseker W, Glownia J, Chollet M, Nelson S, Tono K, Katayama T, Yabashi M, Ishikawa T, Robert A and Grübel G 2014 *Sci. Rep.* **4** 5234
[17] Lee S, Roseker W, Gutt C, Fischer B, Conrad H, Lehmkühler F, Steinke I, Zhu D, Lemke H, Cammarata M *et al.* 2013 *Opt. Exp.* **21** 24647–24664
[18] Yun K, Kim S, Kim D, Chung M, Jo W, Hwang H, Nam D, Kim S, Kim J, Park S Y, Kim K S, Song C, Lee S and Kim H 2019 *Sci. Rep.* **9** 3300
[19] Mancuso A P, Aquila A, Batchelor L, Bean R J, Bielecki J, Borchers G, Doerner K, Giewekemeyer K, Graceffa R, Kelsey O D, Kim Y, Kirkwood H J, Legrand A, Letrun R, Manning B, Morillo L L, Messerschmidt M, Mills G, Raabe S, Reimers N, Round A, Sato T, Schulz J, Takem C S, Sikorski M, Stern S, Thute P, Vagovič P, Weinhausen B and Tschentscher T 2019 *J. Synchrotron Radiat.* **26** 660–676
[20] Lehmkühler F, Dallari F, Jain A, Sikorski M, Möller J, Frenzel L, Lokteva I, Mills G, Walther M, Sinn H, Schulz F, Dartsch M, Markmann V, Bean R, Kim Y, Vagovic P, Madsen A, Mancuso A P and Grübel G 2020 *Proc. Natl. Acad. Sci.* **117** 24110–24116
[21] Madsen A, Hallmann J, Ansaldi G, Roth T, Lu W, Kim C, Boesenberg U, Zozulya A, Möller J, Shayduk R, Scholz M, Bartmann A, Schmidt A, Lobato I, Sukharnikov K, Reiser M, Kazarian K and Petrov I 2021 *J. Synchrotron Radiat.* **28**
[22] Dallari F, Jain A, Sikorski M, Möller J, Bean R, Boesenberg U, Frenzel L, Goy C, Hallmann J, Kim Y, Lokteva I, Markmann V, Mills G, Rodriguez-Fernandez A, Roseker W, Scholz M, Shayduk R, Vagovic P, Walther M, Westermeier F, Madsen A, Mancuso A P, Grübel G and Lehmkühler F 2021 *IUCrJ* **8** 775–783
[23] Dallari F, Reiser M, Lokteva I, Jain A, Möller J, Scholz M, Madsen A, Grübel G, Perakis F and Lehmkühler F 2021 *Appl. Sci.* **11** 8037
[24] Alonso-Mori R, Caronna C, Chollet M, Curtis R, Damiani D S, Defever J, Feng Y, Flath D L, Glownia J M, Lee S, Lemke H T, Nelson S, Bong E, Sikorski M, Song S, Srinivasan V, Stefanescu D, Zhu D and Robert A 2015 *J. Synchrotron Radiat.* **22** 508–513
[25] Liu S, Decking W, Kocharyan V, Saldin E, Serkez S, Shayduk R, Sinn H and Geloni G 2019 *Phys. Rev. Accel. Beams* **22** 060704